

Modeling Omnidirectional Small Antennas for UWB Applications

Stanley Bo-Ting Wang*, Ali M. Niknejad and Robert W. Brodersen
Berkeley Wireless Research Center
Department of Electrical Engineering and Computer Science
University of California, Berkeley, CA 94704
Email: {sbtwang, niknejad, rb}@eecs.berkeley.edu

ABSTRACT

Small antennas are candidates for indoor UWB communication systems operating below 1GHz due to their omnidirectionality and small form factor. The small antennas are modeled as simple circuit networks, and the radiated far fields can be estimated from the voltages across the radiation resistors in the networks. With these models, UWB transmitters and receivers can be designed in circuit simulators in order to facilitate the co-design of the antenna with the radio circuitry without running separate EM simulations.

I. INTRODUCTION

The FCC recently allowed the use of ultra-wideband technology (UWB) transmission in several frequency bands (<960MHz, 3.1~10.6GHz, and 22~29GHz) [1]. This large bandwidth gives rise to some unique advantages such as immunity to multipath fading and high resolution positioning. In the low frequency band, since diffraction around objects is significant and skin depths of objects are relatively large, EM waves are able to reach receivers blocked by obstacles. This promises the possibilities of through-wall communication and imaging. Based on these facts, this paper focuses on antennas for UWB systems operating below 960MHz.

II. CHARACTERISTICS OF SMALL ANTENNAS

For UWB systems working below 960MHz, the free-space wavelength is greater than 30cm, so any antenna of dimension less than ~5cm is deemed as “electrically-small” ($< \lambda/2\pi$). It is believed that applications such as sensor network and portable devices will require such small antennas. These electrically small UWB antennas behave from the input standpoint either as a capacitor or an inductor, i.e., the reactance part dominates the antenna input impedance. This property becomes apparent from exploring the fundamental limit on the radiation quality factor Q of small antennas [2]. The theoretical minimum is $Q = (ka)^{-3} + (ka)^{-1}$, where k is the wave number ($2\pi/\lambda$) and a is the radius of the smallest sphere enclosing the hypothetical radiator. Thus, a smaller antenna yields a larger Q and therefore the impedance is more reactive.

From the circuit perspective, an antenna can be thought of as a lossy one-port network, and power dissipated in the network is equal to the antenna radiation power. For small antennas, since the reactance dominates, they can be assumed to be low loss and realized in either of the two Foster canonical forms [3]. For an antenna operating well below the lowest resonant frequency, the Foster canonical forms circuits reduce to Fig. 1(a)-(b) [3], which enables the use of simple lumped-element circuit models for the study of small antennas.

Another property of small antennas is that they are mostly “*waveform omnidirectional*”, i.e., the waveforms of the radiated E-fields propagating in all directions are the same, and differ only in magnitude. This property is formulated as

$$E(\theta, \phi, R, t) = \alpha(\theta, \phi) \times E(\theta_o, \phi_o, R, t) \quad (1)$$

where R is the observation distance from the antenna, $E(\theta, \phi, R, t)$ is the far-zone E-field propagating in the direction (θ, ϕ) , and $\alpha(\theta, \phi)$ is a direction-dependent scaling factor. This follows because the antenna looks like a “radiating one-point element” in the far-zone.

Since there is only one resistor in each model in Fig. 1 while all the other elements are reactive and dissipate no power, the instantaneous power radiated from the antenna is equal to the instantaneous power dissipated in this resistor, that is,

$$\frac{V(t - \frac{R}{c})^2}{R_{rad}} = R^2 \oint_{4\pi} \frac{E(\theta, \phi, R, t)^2}{\eta_0} d\varpi = R^2 \oint_{4\pi} \alpha(\theta, \phi)^2 d\varpi \times \frac{E(\theta_o, \phi_o, R, t)^2}{\eta_0} = \beta R^2 \frac{E(\theta_o, \phi_o, R, t)^2}{\eta_0} \quad (2)$$

where c is the speed of light, ϖ is the solid angle, η_0 is the free-space characteristic impedance ($=377\Omega$), and β is a constant. From (1) and (2),

$$E(\theta, \phi, R, t) = \pm \frac{1}{R} \sqrt{\frac{\eta_0}{\beta R_{rad}}} \alpha(\theta, \phi) V(t - \frac{R}{c}) \quad (3)$$

Hence, once $\alpha(\theta, \phi)$ is known, circuit designers can scale the time-domain voltage across the radiation resistance in the circuit model and derive waveforms of the radiated E-fields in any direction. A circuit/antenna co-design methodology can then be constructed.

III. MODELING A SMALL DIPOLE ANTENNA

As an example, a co-simulation of a dipole antenna and a simple driving circuit will be given. Assuming the current phasor $I(z)$ on the dipole (Fig. 2) is [4]

$$I(z) = I_m \sin k(h - |z|) \quad (4)$$

Due to symmetry on the horizontal plane, the far-zone E-field does not depend on the azimuthal angle ϕ and can be obtained as

$$E(\theta, \phi) = E_\theta = \eta_0 H_\phi = j \frac{I_m \eta_0 k \sin \theta}{2\pi R} e^{-jkR} \int_0^h \text{sinc}(h-z) \cos(kz \cos \theta) dz = \frac{j60I_m}{R} e^{-jkR} F(\theta) \quad (5)$$

where $F(\theta)$ is the pattern function. When $kh \ll 1$

$$F(\theta) = \frac{\cos(kh \cos \theta) - \cos kh}{\sin \theta} \cong \frac{1 - \frac{1}{2}(kh \cos \theta)^2 - (1 - \frac{1}{2}(kh)^2)}{\sin \theta} = \frac{1}{2}(kh)^2 \sin \theta$$

and yields

$$E_\theta = \frac{j30I_m}{R} e^{-jkR} (kh)^2 \sin \theta = E_{\theta=90^\circ} \sin \theta \quad (6)$$

Equation (6) shows that as long as the operating frequency is low, the far-zone E-fields in all directions only differ from that radiating to $\theta = 90^\circ$ by a scaling factor $\sin \theta$. Therefore, a small dipole antenna is *waveform omnidirectional*.

Fig. 2-4 show the simulated results of a 6cm dipole antenna gain over the elevation angles at different frequencies from a FDTD EM simulator [5]. It can be seen that as long as the frequency is below 1GHz ($h=0.1\lambda$) the magnitude responses only differ by a scaling factor (Fig. 2). After normalization (Fig. 3), the magnitude responses overlap exactly at low frequency region, and the error is less than 0.3dB as frequency goes up to 1GHz. Phase responses also match well (Fig. 4), hence verifying the *waveform omnidirectionality* of small dipoles. If some error ($<3\text{dB}$) is tolerable, this property is valid up to the resonant frequency.

Fig. 5 shows an equivalent circuit of small dipoles derived in [6]. Notice that this topology fits the Foster canonical form shown in Fig. 1(a). For the 6cm dipole, we obtained $C_1 = 0.67\text{pF}$, $C_2 = 0.11\text{pF}$, $L_2 = 7.34\text{nH}$ and $R_{rad} = 294.71\Omega$ by fitting the input impedance of the circuit in Fig. 5 to that calculated by FDTD using a custom optimization tool. The model is then put into the circuit simulator (SPICE) for comparison with EM simulation results. The driving voltage waveform is set to be a 2ns-wide Gaussian function as shown in Fig. 5 with most of its power below 1GHz, and the source resistance is set to 50Ω . The voltage waveform V_{rad} and the far-zone E-field at $\theta = 90^\circ$ at 1m away from the antenna are derived in SPICE and FDTD respectively. After scaling and time shifting, Fig. 6 shows that the two normalized

waveforms match well. The ratio of the peak value of V_{rad} to that of $E_{\theta=90^\circ}$ at 1m before normalization is 2.77. From Eqn. (2), (3), and (6), β is derived and the theoretical ratio of V_{rad} to $E_{\theta=90^\circ}$ at 1m is 2.56, which is within 8% of the simulation results.

Some insights of the antenna behavior can be investigated from the circuit model. According to the model developed above, we can write the transfer function as

$$\frac{E(\theta, \phi, R)}{V_{\text{in}}} = \frac{E(\theta, \phi, R)}{V_{\text{rad}}} \cdot \frac{V_{\text{rad}}}{V_{\text{in}}} = \frac{1}{R} \sqrt{\frac{\eta_0}{R_{\text{rad}}}} \sqrt{\frac{3}{8\pi}} \frac{s^2 L_2 C_1}{s^2 L_2 (C_1 + C_2) + \frac{s L_2}{R_{\text{rad}}} + 1} \cong \frac{1}{R} \sqrt{\frac{\eta_0}{R_{\text{rad}}}} \sqrt{\frac{3}{8\pi}} s^2 L_2 C_1$$

which follows a second-derivative behavioral relation and also gives the magnitude response. Comparing the waveforms of Fig. 5 and Fig. 6, an approximate second-derivative relation can be seen and is consistent with other UWB antenna analyses [7]. This is because the source resistance of 50Ω is much smaller than the dipole impedance so the source voltage is almost equal to V_{in} . The transfer function from source voltage to E-field changes when the source impedance increases. When it is very large, the relation is closer to the first-derivative.

IV. MODELING A LARGE CURRENT RADIATOR

A circuit model was derived for a large-current radiator (LCR) shown in Fig. 7 that was proposed in the early days of the development of UWB and is still utilized [7][8]. FDTD simulation shows that this LCR is also *waveform omnidirectional* at operating frequencies below 1GHz. Because LCR is similar to a loop antenna, electrical properties are expected to follow the circuit model of Fig. 1(b) and are shown in Fig. 8. After curve-fitting the input impedance of the circuit model to that of the LCR, component values are derived as $L_1 = 49.4\text{nH}$, $L_2 = 1.65\text{nH}$, $C_2 = 0.13\text{pF}$, $R_{\text{rad}} = 31\Omega$. Driving the antenna by a step function shown in Fig. 7 with a source resistance equal to 1Ω , the normalized waveforms of V_{rad} from SPICE and E_{rad} at $\theta = 0^\circ$ from FDTD are derived and shown in Fig. 8. Again, the overlap of the waveforms validates the model. The ratio of V_{rad} and E_{rad} is 0.153(m).

V. CONCLUSION

An approach to modeling an omnidirectional small antenna has been proposed. This method transforms an antenna into a circuit model to achieve antenna/circuit co-simulation such that the waveform of the radiated E-field can be designed entirely in the circuit domain. This approach works if the antenna is *waveform omnidirectional*. The procedure is as follows:

1. By inspection, choose one of the simplified Foster canonical forms in Fig. 1.
2. Fit the input impedance of the model with that obtained from the EM simulator.
3. Choose the direction(s) of interest and relate the scaling factor between V_{rad} derived in circuit simulator and E_{rad} derived in EM simulator. Add a voltage-controlled voltage source in the circuit simulator with that scaling factor. The radiated E-field can now be observed in the circuit simulator.

This approach not only provides a way to design UWB interface circuits, but also decouples the circuit design from the EM simulation tools at a very early stage. If some error is tolerable, the working frequency can be extended to the resonant frequency of the antenna.

ACKNOWLEDGEMENT

This work was supported by a ARO grant #065861 and the industrial members of BWRC.

REFERENCES

- [1] FCC Notice of Proposed Rule Making, "Revision of Part 15 of the commission's rules regarding ultra-wideband transmission systems," ET-Docket 98-153.
- [2] J. McLean, "A re-examination of the fundamental limits on the radiation Q of electrically small antennas", *IEEE Trans. on Antennas and Propagation*, Vol. 44, No. 5, pp. 672-676, May 1996.
- [3] S. Ramo, et al., "Fields and Waves in Communication Electronics", John Wiley & Sons, 1994.
- [4] D. Cheng, "Field and Wave Electromagnetics", Addison Wesley, 1989.

- [5] Remcom XFDTD v5.1
- [6] T. Tang, et al., "Equivalent circuit of a dipole antenna using frequency-independent lumped elements", *IEEE Trans. on Antennas and Propagation*, Vol. 41, No. 1, pp. 100-103, Jan. 1993.
- [7] J. Taylor, "Introduction to Ultra-Wideband Radar Systems", CRC Press, 1995.
- [8] Aether Wire and Location, Inc. website <http://www.aetherwire.com>

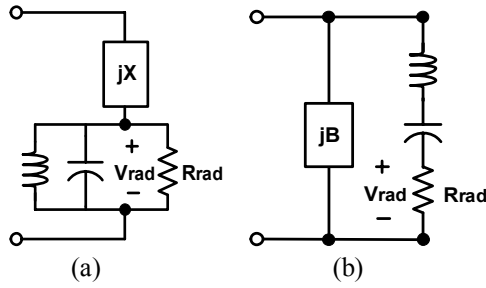


Fig. 1: Equivalent circuits for small antennas.

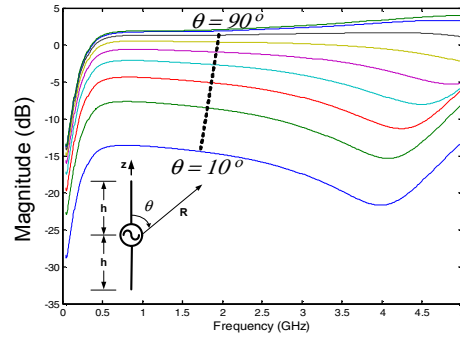


Fig. 2: Magnitude response of 6cm dipole.

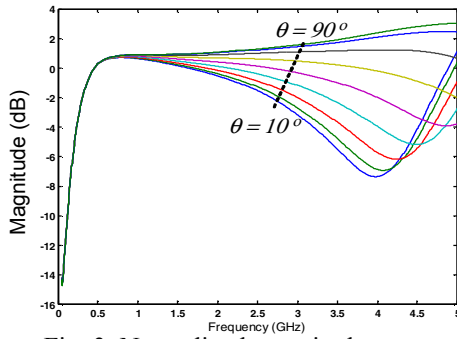


Fig. 3: Normalized magnitude response.

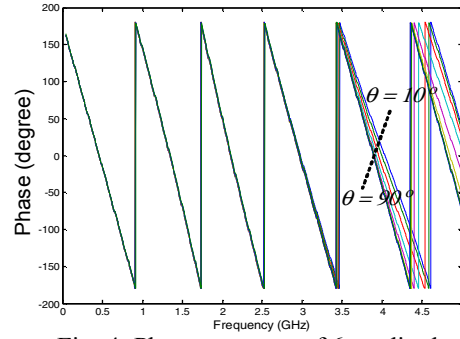


Fig. 4: Phase response of 6cm dipole.

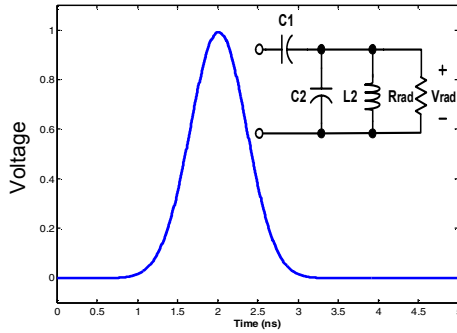


Fig. 5: Dipole model and input voltage waveform.

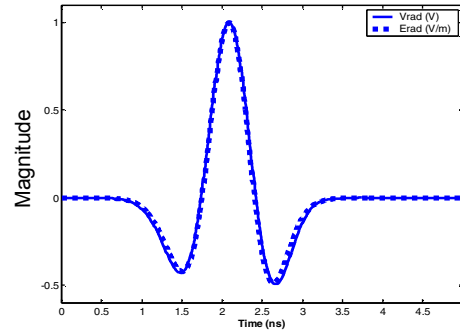


Fig. 6: Normalized V_{rad} and E_{rad} of 6cm dipole.

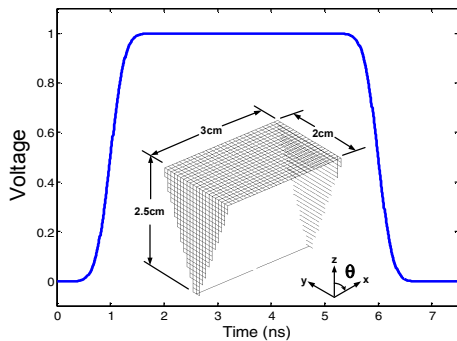


Fig. 7: LCR and input voltage waveform.

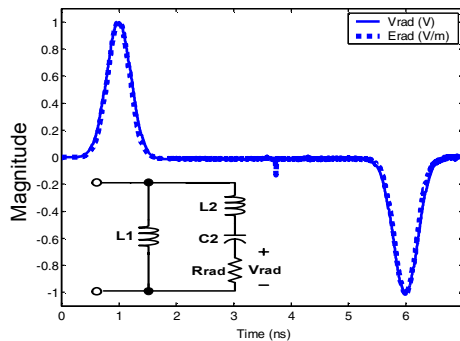


Fig. 8: LCR model and normalized V_{rad} and E_{rad} .